DRB1.3 Third report on UWB channel models

Contractual Date of Delivery to the CEC: T0+36
Actual Date of Delivery to the CEC: November, 2006
Author(s): R. Saadane, A. Menouni Hayar
Participant(s): EURECOM Institute (Mobile Communications Department) (final editing by Giorgio M. Vitetta, CNIT)
Work package: WRPB
Est. person months:
Security:
Nature: Public
Version: V1.1
Total number of pages: 41

Contents

Abstract

The aim of this document it to present an overview of some recent research activities on *ultra–wideband* (UWB) channel modeling. Compared to models introduced in DRB1.2, recent research was focused on more sophisticated tools to model UWB channels, like information theoretic arguments. Physical modeling of UWB channels was also investigated.

1 Introduction

Due to recent developments in digital consumer electronics technology, UWB is becoming more attractive for low cost personal communication applications.

UWB systems are now emerging across a variety of commercial and military applications, including communications, radar, geolocation, and medical systems. First generation commercial wireless UWB products are anticipated to be widely deployed soon. This has been fuelled by a demand for high frequency utilization and a large number of users requiring simultaneous multidimensional high data rate access for applications of wireless internet and e-commerce.

UWB systems are often defined as systems that have a relative bandwidth that is larger than 25% and/or an absolute bandwidth of more than 500MHz (FCC). UWB systems using a large absolute bandwidth are robust to frequency-selective fading, which has significant implications on both design and implementation. Among the important characteristics of the UWB technology are low power devices, accurate localization, a high multipath immunity, low complexity hardware structures and carrier-less architectures [1, 2]. Additionally, the spreading of the information over a very large frequency range decreases the spectral density and makes it compatible with existing systems.

Many researchers are currently working on various projects whose missions are to further explore the potential benefits and future challenges of UWB for extending this technology into the high-rate, multimedia consumer communications [6, 7, 8, 9]. The main objective of this work is to present some recently proposed channel models.

For designing and implementing any wireless system, channel sounding and modelling are a basic necessity. Several studies, theoretical and practical, have shown an extreme difference with respect to narrowband channels [3, 4, 5]. In works about UWB channel modeling researchers are interested in characterizing the path loss law, shadowing, multipath delay spread, coherence bandwidth, average multipath intensity profile and received amplitude distribution of the multipath components ...

The remaining part of this document is organized as follows. A short introduction is provided inn Section 2. Then, the following models are illustrated

1. A modified S-V clustering channel model for the UWB indoor residential environment (Section 3);

2. A path-loss and time dispersion model for indoor UWB propagation (Section 4);

3. An UWB on-body radio channel model based on ray theory and sub-band FDTD methods (Section 5);

4. A comprehensive model for Ultra–Wideband propagation channels (Section 6);

5. An UWB channel model based on sub space analysis (Sections 7 and 8);

6. An UWB channel based on entropy maximization approach (Section 9);

7. An UWB channel model based on the analysis of physical propagation phenomenam (Section 10).

Finally, some conclusions are offered in Section 11.

2 Indoor channel models in the technical literature

Several works about indoor radio propagation measurements and modeling have been proposed so far in the literature. In this report we describe some important contributions, provided in the last two decades, that deal with wideband channel sounding. This is useful to understand the main concepts playing a relevant role in a propagation channel. First of all, we note that propagation/statistical models usually provide a characterization of the following quantities:

- Path loss law;
- Shadowing;
- Multipath delay spread;
- Coherence bandwidth;
- Multipath arrival times;
- Average multipath intensity profile;
- Received amplitude distribution of the multipath components.
- . . .

3 A modified S-V clustering channel model for the UWB indoor residential environment

C.-C. Chong et al. have proposed a new modified *Saleh-Valenzuela* (S-V) clustering channel model based on the measurement data collected in various types of high-rise apartments under different propagation scenarios in the UW) frequency band of 3-10 GHz [11]. A new distribution, namely, a mixture of two Poisson processes, is proposed to model the ray arrival times. This new distribution fits the empirical data much better than the single Poisson process proposed in the conventional S-V model.

3.1 Measurements

Measurements were conducted using a network analyzer transmitting 1601 continuous waves tones uniformly distributed over the 3-10 GHz frequency range. This results in a frequency step of 4.375 MHz and gives a maximum excess delay of about 229.6 ns (i.e., a maximum distance of approximately 68.6 m). The 7 GHz bandwidth gives a temporal resolution of 142.9 ps and the sweeping time is adjusted to sweep across the bandwidth in 800 ms. Calibration was performed in an anechoic chamber with a 1 m reference distance to remove the antenna effects and was saved for post-processing. Measurements were conducted in various types of

high-rise apartments with different sizes, layouts and structures. In each apartment, the *transmitter* (TX) was fixed in the center of the living room, while the *receiver* (RX) was moved throughout the apartment around 8-10 different positions with TX-RX separation ranging from 1 to 20 m. We refer this different RX positions as local points. In order to characterize the small scale statistics of the channel, the RX was moved 25 times around each local point over a 55 square grid with 15 cm spacing between adjacent points. Each point on the grid is referred as a spatial point. Both *line-of-sight* (LOS) and no-LOS (NLOS) scenarios were considered. During the measurements, both TX and RX were fixed at 1.25 m and were kept stationary. In order to confirm the time-invariant nature of the channel and for statistical analysis reliability, at each spatial point, 30 time-snapshots of the complex *channel transfer functions* (CTFs) were recorded. Details about the measurement setup and the environments were reported in [10].

3.2 A Modified S-V clustering channel model

Based upon the apparent existence of clusters in the measurement data, an UWB channel model which accounts for the clustering of *multipath components* (MPCs) is proposed here; it is based on the conventional S-V channel model [22]. The clustering CIR can be expressed as follows:

$$h(t) = \sum_{l}^{L} \sum_{k}^{K} a_{l,k} \delta(t - T_l - \tau_{l,k}) \tag{1}$$

where L is the number of clusters l^{th} cluster, K is the number of MPCs within the $a_{k,l}$ is multipath gain coefficient of the k^{th} component in l^{th} cluster, T_l is the delay of the l^{th} cluster and $\tau_{k,l}$ is the delay of the k^{th} MPC relative to the to the l^{th} cluster arrival time.

The proposed channel model relies on two classes of parameters, namely, inter-cluster and intra-cluster parameters, which characterize the cluster and MPC, respectively.

The distributions of the cluster arrival times, T_l and the ray arrival times, $\tau_{k,l}$ are given by two Poisson processes. According to this model, cluster inter-arrival times and ray intra-arrival times are described by the exponential *probability density functions* (PDFs)

$$p(T_l|T_{l-1}) = \Lambda \exp[-\Lambda(T_l - T_{l-1})], \quad l > 0, \tag{2}$$

and

$$p(\tau_{k,l}|\tau_{k-1,l}) = \lambda \exp[-\lambda(\tau_{k,l} - \tau_{k-1,l})], \quad k > 0, \tag{3}$$

respectively, where Λ is the mean cluster arrival rate and λ is the mean ray arrival rate.

The measurement results show that the single Poisson process given in (3) is insufficient to model the ray arrival times. Thus, we propose to model the ray arrival

times with a mixture of two Poisson processes, so that

$$p(\tau_{k,l}|\tau_{k-1,l}) = \beta\lambda_1 \exp[-\lambda_1(\tau_{k,l}-\tau_{k-1,l})]+(\beta-1)\lambda_1 \exp[-\lambda_2(\tau_{k,l}-\tau_{k-1,l})], \quad k > 0, \tag{4}$$

Here β is the mixture probability, whereas λ_1 and λ_2 are the ray arrival rates. This new model can give an excellent match to the ray arrival times. The average power of a MPC at the delay $T_l + \tau_{k,l}$ is given by

$$\overline{a_{k,l}^2} = \overline{a_{0,0}^2} \times e^{-T_l/\Gamma} \times e^{-\tau_{l,k}/\gamma} \tag{5}$$

where $\overline{a_{0,0}^2}$ is the mean power of the first arriving MPC, Γ is the cluster decay factor and γ is the ray decay factor.

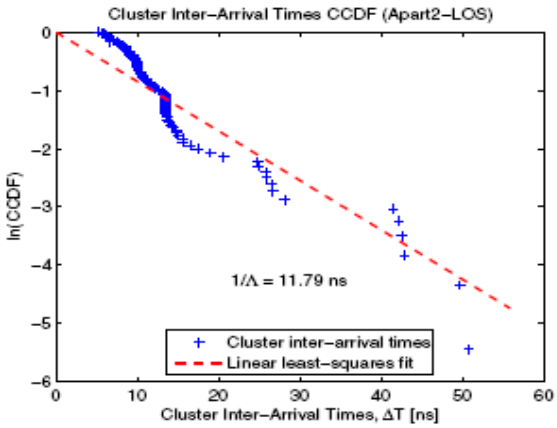

Figure 1: Logarithmic complementary CDF (CCDF) of the cluster inter-arrival times for Apart2 under LOS scenario.

Figures 1, 2, 3 and 4 show the logarithmic *complementary* CDF (CCDF) of the cluster inter-arrival times for Apart2 under LOS scenario, Logarithmic CCDF of the ray intra-arrival times for Apart1 under LOS scenario, normalized cluster relative power versus relative delay for Apart2 under NLOS scenario and the *density functions* (DFs) of the small-scale amplitude fading at different excess delays for Apart1 under NLOS scenario, respectively.

3.3 Conclusions

The model described in this Section is based on a mixture of two Poisson processes and gives an excellent match to the ray arrival times with respect to the single Poisson process proposed in the original S-V model. It was also found that the small-

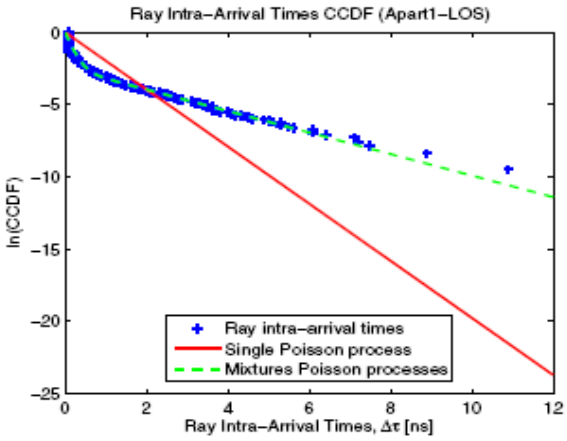

Figure 2: Logarithmic CCDF of the ray intra-arrival times for Apart1 under LOS scenario.

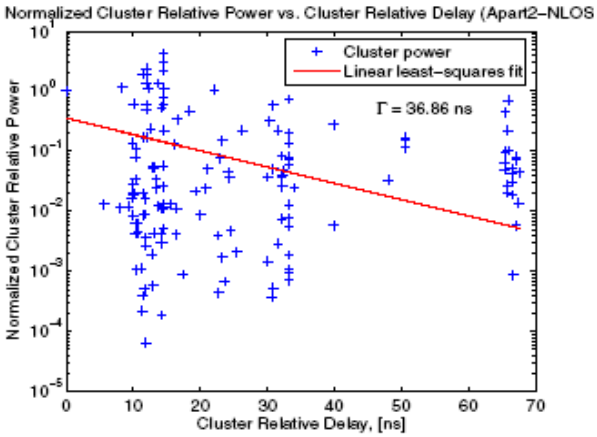

Figure 3: Normalized cluster relative power versus relative delay for Apart2 under NLOS scenario.

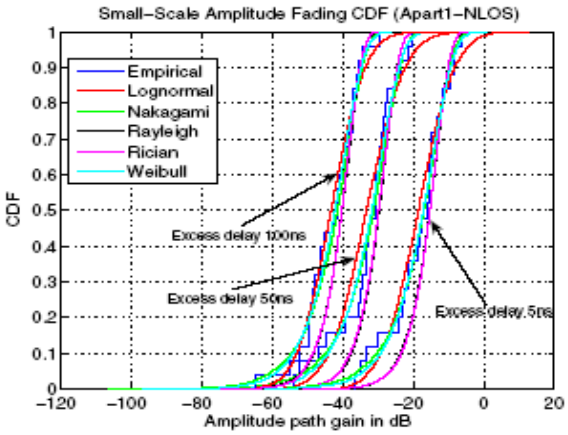

Figure 4: DFs of the small-scale amplitude fading at different excess delays for Apart1 under NLOS scenario.

scale amplitude fading statistics can be well modeled by either the lognormal, Nakagami or Weibull distributions. The parameters of these distributions are relatively invariant across the excess delay and can be modeled by another lognormal distribution.

4 Path-loss and time dispersion model for Indoor UWB Propagation

The propagation of UWB signals in indoor environments is an important issue with significant impacts on the future direction and scope of the UWB technology and its applications. Several approaches to UWB channel characterization perform propagation measurements in the frequency domain and convert the results to the time domain by means of Fourier processing.

Channel measurements provide the high resolution necessary for the development of accurate UWB communication channel models. In the work described in [20] higher solution pulses used in the measurements; these are good candidates for small cell scenarios, such as single-cell-per-room where few obstructions exist.

4.1 Measurements

Time-domain measurements were performed using a sampling oscilloscope as receiver and a Gaussian-like pulse generator as a transmitter. Two low-noise wideband amplifiers were used at the receiver side. Each amplifier has a gain of 10 dB

and a 3 dB-bandwidth of 15 GHz. The width of the excitation pulse is less than 100 ps. Offset calibration is carried out with a matched load before performing any measurement. The received signals were sampled at a rate of 1 sample per 10 ps. An acquisition time window of 100 ns was selected to ensure that all the observable multipath components are accounted for. This time window is consistent with the maximum excess delay of 70 ns reported by other investigators [21]. The sampling oscilloscope allows a maximum of 5K points at a time. The 5K points correspond to a 50 ns time window. Two measured 50 ns time windows were cascaded to yield a 100 ns acquisition time. A total of about 400 profiles were collected. The spatial width of the used pulse in our measurements is much smaller than the one used in previously published measurements and is small enough to make the line-of-sight path always resolvable from any other multipath component. Information about the excitation pulse allows to perform a deconvolution and hence lead to a generalization of results for use in other communication applications in the covered frequency ranges [44].

4.2 Small-scale fading and signal quality

The observations of received signals at different points in a measurement grid confirm the absence of small-scale fading. To quantify this effect, let us consider the signal quality parameter defined as [20]:

$$Q = 10 \log 10 \left(\frac{E}{E_0} \right) \tag{6}$$

where E is the received signal energy given by

$$E = \int_0^T r^2(t) dt \tag{7}$$

and $r(t)$ is the received signal.

Robustness of UWB communication systems, insofar as multipath is concerned, is manifested by small variations in signal quality at various grid locations [20].

4.3 Path-loss and large-scale analysis

The energy in the received profile decreases with the distance between the receiver and the transmitter. The path-loss exponent, n, is a measure of the decay in signal power with distance, d, according to $1/d^n$. A reference measurement is performed at a distance of 1 m from the transmitter. Subsequent energy measurements are performed with respect to the reference measurement. Using the log-normal shadowing assumption, the path-loss exponent, n, is related to the received energy at distance d and the reference measurement by:

$$PL(d) = \bar{PL}(d_0) + 10n \log_{10}(\frac{d}{d_0}) + X_\sigma \tag{8}$$

The extracted parameters for LOS and NLOS scenarios are summarized in Table 1 in [20]. The minimum path-loss exponent is 1.27 for the case of a narrow corridor which has nearly the behaviour of a lossy waveguide structure. The maximum path-loss exponent is 3.29 in some obstructed scenarios. The global LOS parameters are $n = 1.61$ and $\sigma = 1.58$ dB for the TEM horns and $n = 1.58$ and $\sigma = 1.91$ dB for the biconical antennas. The NLOS scenarios have path-loss exponents larger than 2 and also have larger σ values compared with LOS scenarios. In general, there is close agreement between the results obtained with directive antennas and the results obtained with omni-directional antennas. This similarity of results obtained with the two types of antennas de-emphasizes the contribution of the back reflection components. Some UWB frequency domain measurements were also performed around 5 GHz [20], which is close to the center frequency in the spectrum of the pulse used in our experiments. The extracted parameters are $n = 1.7$, $\sigma = 1.6$ dB for LOS scenarios and $n = 3.5$, $\sigma = 2.7$ dB for NLOS scenarios.

4.4 Time dispersion results

Time dispersion parameters shed some light on the temporal distribution of power relative to the first arriving components. Delay spreads restrict transmitted data rates and could limit the capacity of the system when multi-user systems are considered. The time dispersion of UWB pulses can be presented as the ratio of the average arrival time to the spread of the arrival time. The formulation of time dispersion parameters is given in [38]. Scatter plots analysis of UWB measured data in [20] indicates that there is no relationship between delay spread and *transmitter-receiver* (T-R) separation. This is in agreement with that reported in [38] and [22] for narrowband systems. On the other hand, when considering the relationship between the received energy and the delay spread, lower energy signals seem to suffer from a larger excess delay. However, this is because the locations where the received energy is low are usually obstructed and signals arrive at the receiver through many paths. In general, received power is not correlated with the excess delay parameters. In [38] and [22] too, scatter plots of τ_{rms} delay spread versus path-loss indicate no correlation.

4.5 Conclusion

UWB channel measurements and the corresponding statistical analysis have evidenced that, unlike narrowband signals, UWB signals are immune to multipath fading. The calculated path-loss exponent was as low as 1.27 for a narrow corridor. For LOS and NLOS scenarios the global path-loss exponents were found to be nearly 1.6 and 2.7, respectively. The calculated time dispersion parameters for the measured results indicate high concentration of power at low excess time delays.

5 UWB on-body radio channel modelling: ray theory and sub-band FDTD analysis

Conventional and empirical channel models available for many narrowband and wideband systems are insufficient to describe the channel behavior due to the UWB nature of the transmitted signals. The *ray tracing* (RT) technique and *finite difference time domain* (FDTD) methods have been widely studied and applied to indoor/outdoor propagation modelling for narrowband and UWB systems. Sarkar et al presented a survey of various propagation models for mobile communications [24]. Wang et al introduced a hybrid technique based on the combination of RT and FDTD methods for narrowband systems [25]. Recently, Attiya et al proposed a simulation model for UWB indoor radio channels using RT [26]. For UWB on-body radio channel modeling, Fort et al simulated pulse propagation around the torso at the frequency range 2 - 6 GHz using **Remcom XFDTD** [27]. However, the variation of UWB on-body channel at different frequencies caused by material dispersion was not taken into account.

Zhao et al [30] presented a novel deterministic on-body channel model using a sub-band FDTD method.

5.1 Two-dimensional on-body propagation channels

Some path-loss results along the trunk[1] were acquired using the sub-band FDTD method, the UTD/RT method and measurement. Good agreement is achieved when the creeping distance of the transmitter and receiver is small. However, when the distance approaches the maximum, ripples are observed from UTD/RT and measurement, which are caused by the adding up or canceling of two creeping rays traveling along both sides of the elliptical 'trunk'. The sub-band FDTD model fails to accurately predict such phenomenon due to the staircase approximation of the curved surfaces and such a problem can be alleviated by using a conformal FDTD method [29]. Using the same antenna at different receiver locations, for PICA, sub-band FDTD provides more accurate results (in terms of the number of multipath components) than UTD/RT compared with measurement since FDTD can fully account for the effects of reflection, diffraction and radiation, while some rays are missing in UTD/RT model compared with measurement.

Other results about the on-body radio channel modeling can be found in [30].

5.2 Three-dimensional on-body propagation channels

Both the sub-band FDTD and UTD/RT are applied to model the UWB on-body radio channel in three dimensions.

[1] A support where we mounted a 2-D ellipse cylinder used for modeling both transmitter and receiver.

5.3 Conclusion

An on-body radio channel modeling was performed using a sub-band FDTD and a combined UTD/RT model. In the sub band FDTD model, the entire frequency band (3 - 9 GHz) was first divided into 12 sub-bands with 500 MHz bandwidth for each sub-band in order to take into account the material frequency dispersion at different frequencies. Within each sub-band, the conventional FDTD was applied to estimate the channel impulse response. A combination technique is used at the receiver to recover all the sub-band simulations. The advantage of this method is its ability of modeling materials with any type of frequency dependence. In the UTD/RT model, the human body is approximated by a conducting sphere and cylinders, and the ray tracing technique is used together with the generalized Fermat principle to find surface diffracted ray path while the UTD surface diffraction coefficients are used for calculating the received signal strength. The proposed models are applied to both 2-D and 3-D on-body scenarios and compared with measurement results. For cases in which both transmitter and receiver are mounted on the trunk, UTD/RT provides relatively simple and reliable solutions even if the human body is modeled as a conducting elliptic cylinder; while for more complicated scenarios as like for the whole body channel modeling, the sub-band FDTD is capable of providing more general solutions due to its ability of fully accounting for the effects of reflection and diffraction. The modeling results indicate that the antenna pattern has a significant impact on on-body radio channels. Through the UTD/RT approach, the effect of different antenna types on on-body radio channels is also investigated. The modeling results show good agreement with measurement.

6 A Comprehensive model for ultra–wideband propagation channels

Recently, Molisch et al. [31] have provided a comprehensive statistical model for UWB propagation channels that is valid for a frequency range from 3 to 10 GHz. It is based on measurements and simulations in the following environments: residential indoor, office indoor, built-up outdoor, industrial indoor, farm environments, and body area networks. The model is independent of the used antennas. It includes the frequency dependence of the path-loss, as well as several generalizations of the Saleh-Valenzuela model, like mixed Poisson times of arrival and delay dependent cluster decay constants. The model can thus be used for realistic performance assessment of UWB systems. It was accepted by the IEEE 802.15.4a *working group* (WG) as a standard model for evaluation of UWB system proposals.

6.1 Generic channel model

6.2 Environments

The following environments are very important for sensor network applications, and are the ones for which the model is parameterized:

- Indoor residential.
- Indoor office.
- Outdoor.
- Industrial environments.
- Agricultural areas/farms.
- Body-area network (BAN).

The measurements and simulations that form the basis of the model in the different environments cover different frequency ranges.

6.3 Path gain

We define the frequency-dependent path gain (related to wideband path gain [32, 33]) in a UWB channel as:

$$G(f,d) = E\left[\int_{f-\Delta f/2}^{f+\Delta f/2} |H(\tilde{f},d)|^2 d\tilde{f}\right] \tag{9}$$

where $H(f,d)$ is the transfer function from antenna connector to antenna connector, the frequency interval Δf is chosen small enough so that the diffraction coefficients, the dielectric constants, etc., can be deemed constant within that bandwidth, d is the distance between the transmitter and the receiver, and the expectation E is taken over the small-scale and large-scale fading. The total path gain shows random variations (due to shadowing), which are log-normally distributed:

$$G = G_0 - 10n\log_{10}\left(\frac{d}{d_0}\right) + S \tag{10}$$

where S is a Gaussian-distributed random variable with zero mean and a standard deviation σ_S.

6.4 Power delay profile (PDP)

The impulse response (in complex baseband) of the S-V (Saleh-Valenzuela) model is given by [22]

$$h_{discr}(t) = \sum_{l=l}^{L}\sum_{k=1}^{K} a_{l,k} e^{j\phi_{k,l}} \delta(t - T_l - \tau_{l,k}) \tag{11}$$

where $a_{k,l}$ is the tap weight of the k^{th} component in the l^{th} cluster, T_l is the delay of the l^{th} cluster, $\phi_{k,l}$ is the delay of the k^{th} MPC relative to the l^th cluster arrival time T_l. The phases $\tau_{k,l}$ are uniformly distributed, i.e., for a bandpass system, each of them is taken as a uniformly distributed random variable in the range $[0, 2\pi]$. Deviating from the standard SV model, the number of clusters L is modeled as Poisson-distributed with probability density function (pdf)

$$pdf_L(L) = \frac{\bar{L}^L \exp(-\bar{L})}{L!} \tag{12}$$

The distributions of the cluster arrival times are given by a Poisson processes (see Paragraph 3.2).

The PDP (mean power of the different paths) is exponential within each cluster

$$E\{|a_k, l|^2\} \propto \Omega_l \exp(-\tau_{k,l}/\gamma_l) \tag{13}$$

where Ω_l is the integrated energy of the l^{th} cluster, and γ_l is the intra-cluster decay time constant.

The cluster decay rates are found to depend linearly on the arrival time of the cluster, i.e.

$$\gamma_l \propto k_\gamma T_l + \gamma_0 \tag{14}$$

For the NLOS case of some environments (office and industrial), the shape of the power delay profile can be different, namely (on a log-linear scale)

$$E\{|a_k, l|^2\} \propto (1 - \chi . \exp(\tau_{k,l}/\gamma_{rise})) . \exp(\tau_{k,l}/\gamma_1) \tag{15}$$

Here, the parameter χ describes the attenuation of the first component, the parameter γ_{rise} determines how fast the PDP increases to its local maximum, and γ_l determines the decay at later times.

6.5 Small-scale fading

The distribution of the small-scale amplitudes is Nakagami

$$pdf(x) = \frac{2}{\Gamma(m)} (\frac{m}{\Omega})^m x^{2m-1} \exp(-\frac{m}{\Omega} x^2) \tag{16}$$

where $m \geq 1/2$ is the Nakagami m–factor, $\Gamma(m)$ is the gamma function, and Ω is the mean-square value of the amplitude. A conversion to a Rice distribution is approximately possible [34]. The m parameter is modeled as a lognormally distributed random variable, whose logarithm has a mean m_0 and standard deviation σ_{m_0}. For the first component of each cluster, the Nakagami factor is modeled differently. It is assumed to be deterministic and independent of delay

$$m = \tilde{m_0} \tag{17}$$

Table 1: PATHLOSS MODEL FOR BAN.

Parameter of BAN	Value
γ	107.8 dB/m
d_0	0.1 m
G_0	-35.5 dB/m

The parameters of the model are extracted fitting measurement data to the model described previously. In residential environments these parameters where extracted form measurements that cover a range from 7 to 20 m, up to 10 GHz [11]. For office environments, the model was based on measurements that cover a range from 3 to 28 m, in the frequency interval 2 - 8 GHz [28]. For outdoor, the measurements cover a range from 5 to 17 m, in the frequency interval 3 - 6 GHz [28].

The derivation of the model and a description of the simulations for the farm area can be found in [36]. The model for industrial environments was extracted from measurements [34] that cover a frequency range from 3 to 10 GHz and a distance range from 2 to 8 m, though the path-loss also relies on values from the literature [38]. The tables in [51] summarize the values of the parameters described mentioned in this paragraph.

Simulations and measurements of the radio channel around the human body indicate that some modifications are necessary to accurately model a *body area network* (BAN) scenario. Due to the extreme close range and the fact that the antennas are worn on the body, the BAN channel model has different path loss, amplitude distribution, clustering, and inter-arrival time characteristics compared with the other application scenarios within the 802.15.4a context. In the BAN context the path gain can be calculated according to the following formula

$$G_{dB} = -\gamma(d - d_0) + G_{0,dB} \tag{18}$$

The impulse responses in different environments show some noticeable differences. The typical impulse response in a residential NLOS situation (CM2) evidences a clear separation between the MPCs, and the arrival in clusters. This arises from the use of the SV model (with modified MPC arrival statistics) as described previously. In strong contrast to this are the impulse responses in an industrial NLOS environment. In this case, it was found that the first arriving MPC is strongly attenuated, and the maximum in the instantaneous power delay profile $|h(\tau)|^2$ occurs only after about 50 ns. This is especially significant for ranging geolocation applications, since the ranging requires the detection of the first path, not of the strongest path. Detection of such a weak component in a noisy environment can be quite challenging.

7 Sub space analysis for modeling UWB channel

7.1 Introduction

Based on UWB channel measurements conducted at Eurecom Institute [5] an UWB channel model is developed. This UWB channel model aims at characterizing the second order statistics of indoor Ultra-Wideband (UWB) channels using channel sounding techniques. These are based on a eigen-decomposition of the channel auto–covariance matrix, which allows for the analysis of the growth in the number of significant degrees of freedom of the channel process as a function of the signaling bandwidth as well as the statistical correlation between different propagation paths.

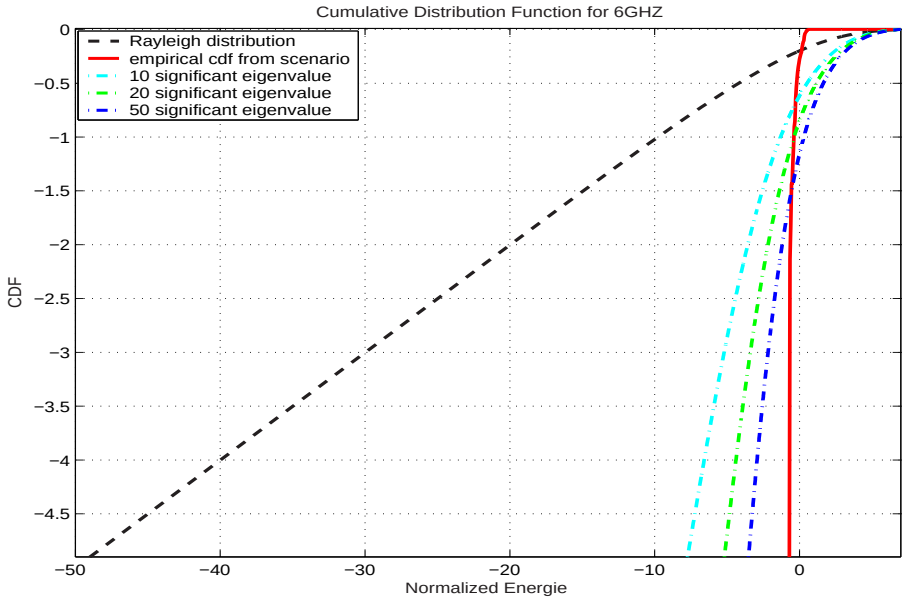

Figure 5: Cumulative distribution function of the energy in an UWB scenario.

Figure 5 (extracted from [39]) shows the cumulative distribution function of the total received energy over a UWB channel of 6 GHz bandwidth in comparison to a flat fading Rayleigh channel with the same average received energy. The measurements were conducted in a typical office environment. The Cumulative Distribution Function (CDF) corresponding to the UWB channel is very close to a step function, which proves that the received energy is effectively constant irrespective of channel realization. The physical explanation for this behavior comes from the fact that the large bandwidths considered here (> 1 GHz) provide a high temporal resolution and enable the receiver to resolve a large number of paths of the impinging wave front. Provided that the channel has a high diversity order (i.e., we have a rich multipath environment), the total channel gain is slowly varying compared to its constituent components. It has been shown [45, 46] through measurements that, in indoor environments, the UWB channel can contain several hundreds of paths of significant

strength.

Based on the observation of UWB channel energy behaviour, authors in [39] were interested on a sub space channel analysis. This allows to evaluating the number of UWB channel independent multipaths.

7.2 Results

A model based on a sub-space analysis has been developed. The results have shown the evolution of the number of channel eigenvalues as a function of the system bandwidth for both LOS and NLOS scenarios. This has lead to the conclusion that the number of eigenvalues tends to saturate for the extreme bandwidth of UWB systems. This seems to suggest that all significant multipath components can be resolved. Moreover, the results have shown that there is a strong statistical dependence among paths coming from different clusters. This in contrast with most propagation models.
An important result obtained in this analysis is that the number of *degrees of freedom* (DoF) does not scale linearly with the bandwidth. This number is dependent on the environment and the channel settings.
A study is provided to confirm the results in [39]. It is based on the information theoretic aspects using *Akaick information criterion* (AIC) and *minimum description length* (MDL) criterion [54]. A recent research have also shown a sublinear scaling of UWB number of DoF versus the bandwidth and computed the capacity penalty due to this sublinear behavior [59].

7.3 Conclusion

The model presented in [39] is based on sub-space channel analysis. This study has resulted in some important results about the channel energy behavior and about the number of independent multipaths.

8 Ultra–wideband channel modeling on the basis of information-theoretic criteria

8.1 Model selection procedure

The main objective of the model selection procedure is to choose the distribution that minimizes the discrepancy among all members of the candidate set [16]. The model selection methodology can be used to characterize multivariate distributions; in practice, however, this is hardly feasible because of the large bandwidth and the resulting large number of taps.
In [12] Schuster and Bolcskei used Akaikes Information-Theoretic Criteria to determine suitable distributions for UWB channel impulse response taps. Denote the unknown cumulative distribution function (CDF) of the operating model by F, and

the set of all CDFs by $\mathcal{M}$. A parametric candidate family $\mathcal{G}^j = \{G^j_{\Theta^j} | \Theta^j \in \mathcal{T}^j\}$ is the subset of $\mathcal{M}$, with individual CDFs G^j_Θ. parametrized by the U -dimensional vector $\Theta^j \in \mathcal{T}$, with $\mathcal{T}^j \subset \mathrm{R}^U$. In model selection using AIC, The AIC is an approximately unbiased estimator of the expected Kullback-Liebler (KL) distance

$$AIC_j = -2 \sum_{n=1}^{N} \log g^j_{\hat{\Theta}}(x_n) + 2U \tag{19}$$

with $\hat{\Theta}^j$=arg $\max_{\Theta^j \in \mathcal{T}^j} \frac{1}{N} \sum_{n=1}^{N} \log g^j_{\hat{\Theta}}(x_n)$, the Akaike weights are given by

$$\omega_j = \frac{e^{-\frac{1}{2}D_j}}{\sum_{i=1}^{J} e^{-\frac{1}{2}D_i}} \tag{20}$$

with $D_j = AIC_j$ – min AIC_i and $i \in J$.

The candidate set C thus consists of the single-parameter $(U = 1)$ Rayleigh family and the two parameter $(U = 2)$ Rice, Nakagami, lognormal, and Weibull families. The Rice, akagami, and Weibull families contain the Rayleigh family as a special case. Rayleigh, Rice, and Nakagami amplitude distributions can be justified from physical principles [44]. The Weibull [17] and lognormal [19], [18] distributions seem to lack physical support for small-scale fading [44].

8.2 Results

In [12] AIC is applied to measurement data to evaluate the different tap amplitude distributions put forward in the UWB literature. The candidate set C thus consists of the single-parameter $(U = 1)$ Rayleigh family and the two parameter $(U = 2)$ Rice, Nakagami, lognormal, and Weibull families. The Rice, akagami, and Weibull families contain the Rayleigh family as a special case. Rayleigh, Rice, and Nakagami amplitude distributions can be justified from physical principles [44]. The Weibull [17] and lognormal [19], [18] distributions seem to lack physical support for small-scale fading [44].

In [12] for MCI: Fig. 1 shows the normalized empirical power delay profile (PDP) of the measured channel for the first 800 taps, along with the Akaike weights for each candidate family.

- The Rayleigh distribution shows the best fit, followed by the Rice, Nakagami, and Weibull distributions in no particular order.
- The lognormal distribution shows a consistently bad fit, with the exception of a few isolated taps.
- The variability of the Akaike weights is high across taps.

For MCII: Fig. MCII depicts the normalized empirical PDP and the Akaike weights obtained from the time-domain measurement campaign.

- The Ricean distribution shows the best fit for the first 1200 taps.
- The Rayleigh distribution fits well for 1200 taps .
- The lognormal distribution does not fit the measurements at all, while the Nakagami distribution is suitable only for the first few taps.
- The Weibull distribution shows a good fit for some taps.

The analysis shows that even for bandwidths of up to 3 GHz Rayleigh and Rice distributions provide a good fit, although the differences of the Akaike weights for the Nakagami and Weibull distributions are often small, especially in MCI. Consequently, the data do not provide enough evidence to unequivocally select a single distribution. However, the empirical support for Rayleigh and Rice fading, combined with the mathematical tractability of these distributions, leads us to advocate their use.

Degrees of Freedom: Results about DoF scaling behavior for different captured energy percentage as a function of W is presented. The scaling is approximately linear in all cases.

Taps correlation: On average, the correlation is small, but some taps show strong correlation. In the NLOS setting, the correlation is somewhat higher in general.

Entropy: A figure about $\hat{H}$ shows, however, that with a gap of up to 1 nat. Thus, even though the intertap correlation is often low, it is not negligible in its effect on the empirical entropy, so that we cannot conclude that the taps are essentially uncorrelated.

Capacity: The result for the NLOS setting, along with the capacity of the AWGN channel with the same receive SNR, is shown in figure about the capacity $\hat{C}$, where we set P/N_0 = 10 dB, and used K = 5608 tones at W = 3 GHz. The channel synthesized according to the uncorrelated Ricean model predicts the ergodic capacity of the measured channel very accurately, with a maximum error at P/N0 = 10 dB of less than 0.3% in the NLOS setting, less than 0.2% in the OLOS setting, and less than 0.07% in the LOS setting. The small gap between the capacity of the measured and synthesized channels can be attributed to the lack of correlation between taps in the synthetic channel, and the remaining differences between the Ricean tap distributions and the operating model.

Mutuel Information: The Mutuel Information study shows the empirical CDF of the mutual information I, estimated for the measured and the synthesized channels. The slope of the CDF for the synthetic channel is higher than the slope of the corresponding CDF for the measured channel, an effect that can be attributed to the intertap correlation in the measured channel. For small outage probabilities, the

outage capacity predicted by the uncorrelated Ricean model is significantly higher than the outage capacity obtained from the measurements.

On the basis of indoor UWB channel measurements in the frequency band from 2 GHz to 5 GHz, the AIC support Raleigh respectively Ricean tap amplitude distributions is founded. This is somewhat surprising, as it is often argued that for large bandwidths the number of partial waves contributing to each tap is not high enough to justify the complex Gaussian assumption by the central limit theorem. The number of significant eigenvalues of the channel impulse response covariance matrix scales approximately linearly with bandwidth. Consequently, the diversity order of the channel shows the same scaling behavior, a common assumption in information-theoretic studies of UWB systems. Nevertheless, its found that there seems to be correlation between the individual channel taps, thus invalidating the discrete-time assumption US.

8.3 Conclusion

As a finale conclusion about this model: Model selection using AIC shows that Rayleigh, Rice and Weibull distributions exibit a good fit for the measurements.

9 A maximum entropy approach to ultra-wideband channel modeling

In [40] a unified framework for Ultra-Wideband channel (UWB channel) modeling based on the maximum entropy approach is provided. The main goal of this model is to analyze how channel uncertainty scales with bandwidth in UWB systems. Equivalently, the number of parameters necessary to predict the wideband channel is determined. The channel model is derived based the maximum entropy approach and validated through measurements performed at Institut Eurecom.

9.1 Maximum entropy modeling (MEM)

The wireless channel suffers from constructive/destructive interference signaling and therefore yields a randomized channel for which one has to attribute a joint probability distribution for the channel frequency response. The basic idea in the channel model proposed in [40] is based on the response of the question:

Question: Knowing only certain informations related to channel (power, measurements), how to translate that information into a model for the channel?

Response: This question can be answered in light of the Bayesian probability theory [41] and the principle of maximum entropy.

9.2 Maximum entropy modeling (MEM) for channel power knowledge

In the case that the modeler knows however that the channel carries some power P and is stationary during the channel modeling phase.
The power delay spectrum is defined as

$$P(\tau) = \sum_{k=-\infty}^{\infty} R(k) e^{j2\pi\tau k} \tag{21}$$

where $\tau = \hat{\tau}/T_s$ is the normalized delay and $\hat{\tau}$ is the delay in seconds.

The spectral autocorrelation function is defined as:

$$R(k) = E[h_i h_{i+k}^*] \tag{22}$$

where $\{h_i\}_{i\in Z}$ be the sequence of samples at frequencies $i\delta_f$ (δ_f is the frequency resolution) of the channel frequency response.

For a Gaussian random process, with power delay spectrum $P(\tau)$, the entropy H is given by

$$H = \log(\pi e) + \int_{-1/2}^{1/2} \log(P(\tau) + \epsilon) d\tau \tag{23}$$

To maximaze H the Lagrange multipliers with respect to R(k) is used [40].

$$C = H - \mu_0 \left(\int_{-\tau_{max}/2}^{\tau_{max}/2} P(\tau) d\tau - P \right) \tag{24}$$

If there is no knowledge except the maximum delay, the model gives an infinite number of clusters and the power is equally split across the different clusters. The methodology can be easily extended if the modeler has knowledge of the bandwidth (which determines the number of correlation coefficients $R(k)$) used.

9.3 MEM for covariance channel knowledge

The others in [40] they suppose that the modeler has knowledge (through measurements) of a finite number of frequency autocorrelation coefficients R(k). The number of coefficients is determined by the measured bandwidth as well as the measurement resolution. The estimated entropy is given by:

$$\hat{H}^N = \log(\pi e) + \int_{-1/2}^{1/2} \log \frac{\sigma^2}{|1 + \sum_{k=1}^{N} a_k^{(N)} e^{i2\pi k\tau}|^2} \tag{25}$$

The coefficients $a_1, a_2, ..., a_N$, σ^2 are obtained by solving the Yule-Walker equations

$$R(0) = -\sum_{k=1}^{N} a_k R(-k) + \sigma^2 \tag{26}$$

$$R(l) = -\sum_{k=1}^{N} a_k R(l-k), \quad l = 1, ..., N. \tag{27}$$

The estimated entropy in equation (25) is based on AR-modeling of the spectral autocorrelation function $R(k)$.

9.4 Entropy maximization results

The scaling of channel uncertainty with respect to the bandwidth is analyzed. As one can observe in figure 6, the channel uncertainty decreases with bandwidth. However, in the Gaussian case, additional information provided by the frequency samples does not lower the uncertainty as the samples are completely independent. The results show that with increasing bandwidth, one is certainly able to capture the small variations.
In the UWB channel model based on Entropy maximization approach, the others show that the entropy is a useful measure and the slope decrease characterizes how information scales with bandwidth. In particular, in wideband schemes, they have shown that it is possible to reproduce the channel frequency behavior with a limited number of coefficients since the channel uncertainty decreases with bandwidth.

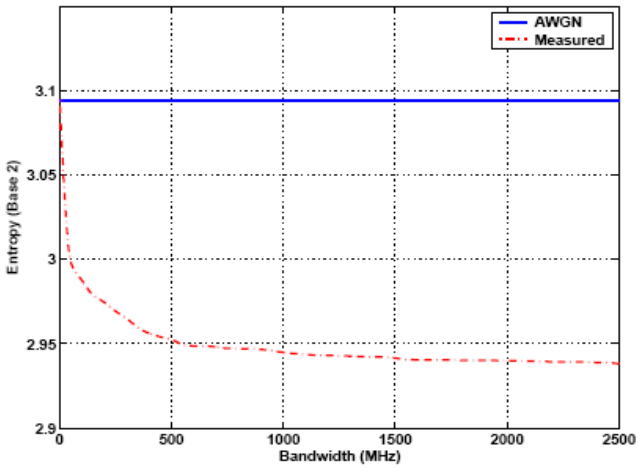

Figure 6: Entropy variation with respect to the bandwidth.

10 A UWB channel model based on an physical analysis of propagation phenomena

The ultimate performance limits of any communications system are determined by the channel it operates in. For a UWB system, this is the UWB propagation channel, which differs from conventional (narrowband) propagation in many respects. The performance of a system thus can only be evaluated when realistic channel models are available.
The UWB impulse response is the result of the superposition of several MPCs. As a first step towards our new channel model we investigate the properties of a single MPC. Qiu [47] presented the impact of large bandwidths on the impulse response due to diffraction. Based on a heuristic approach he proposed a model to show the relationship between delay spread and large bandwidths. In [55, 56] the reflection mechanisms for an UWB channel was analysed, using the *time domain channel impulse response* (TD-CIR) expression derived by Barnes in [49] and based on the analysis of the expression of the reflection coefficient versus frequency.

10.1 Analysis of the UWB impulse response

The UWB impulse response is the result of the superposition of several MPCs. As a first step towards our new channel model we investigate in the properties of a single MPC. Qiu [48] presented the impact of large bandwidths on the impulse response due to diffraction. Based on a heuristic approach he proposes a model showing the relationship between delay spread and large bandwidths. In the sequel, we will analyze the reflection mechanisms for a UWB channel.

Using the expression of the reflection coefficient versus the frequency, Barnes [49] derived a TD-CIR expression. In [48], Qiu derived the TD-CIR due to diffraction for a perfectly conducting half-plane.

The expression of the reflection coefficient versus the frequency and the incident angle, $R(\psi, s)$ expressed as

$$R(\psi, s) = \pm \frac{\sqrt{s + 2a} - \kappa\sqrt{s}}{\sqrt{s + 2a} + \kappa\sqrt{s}} \tag{28}$$

with $\tau = \frac{\sigma}{\epsilon}$, $\beta = \frac{\sqrt{\epsilon_r - cos^2\psi}}{\epsilon_r sin\psi}$, $a = \tau/2$, $\kappa = \beta$ for vertical polarization and $a = \tau/2$, $\kappa = (\epsilon_r\beta)^{-1}$ for horizontal polarization.
Barnes [49] derived the time domain expression of $r(t)$ as

$$r(t) = \left[K\delta(t) + \frac{4\kappa}{1-\kappa^2}\frac{\exp(-at)}{t}\sum(-1)^{n+1}nK^nI_n(at)\right] \tag{29}$$

Qiu in [48] derived the time domain impulse response due to diffraction for

perfectly conducting half-plane as follow

$$h_d(\tau) = \frac{\sqrt{2r/c}}{2\pi}\left[\frac{cos\frac{1}{2}(\varphi-\varphi_0)}{\tau+\frac{r}{c}cos(\varphi-\varphi_0)} - \frac{cos\frac{1}{2}(\varphi+\varphi_0)}{\tau+\frac{r}{c}cos(\varphi+\varphi_0)}\right]\frac{1}{\sqrt{\tau-r/c}}U(t-r/c) \quad (30)$$

where c is the speed of light, τ is the path delay, φ and φ_0 are defined as shown in Figure 7.

Figure 8 shows the effect of the material constitutive parameters (ϵ: permittivity and σ: conductivity) on TD-CIR for a bandwidth equal to 1 GHz.

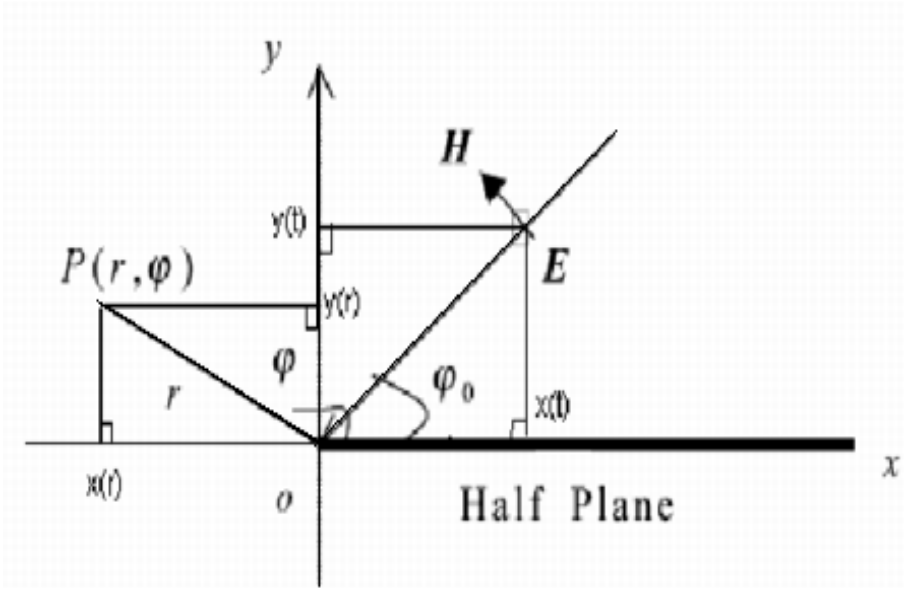

Figure 7: Diffraction at a perfectly conducting half-plane.

As it can be inferred from from this figure, the impulse response of a single MPC may show significant dispersion. These results clearly demonstrate that a single path of an UWB channel can experience a dramatic dispersion effect in time domain in the range of several nanoseconds. If we further recall that the RMS delay spread τ_{rms} for UWB channels ranges from 5 ns to 25 ns for indoor CM1-CM4 environments [50], this dispersion should be taken into account to model UWB path response.

This implies that, the UWB impulse response should not be represented by a set of Dirac functions. The large dispersion in time domain may also explain parts of the clustered behavior of the Power Delay Profile (PDP) observed in many UWB channel measurement campaigns [39, 50]. This statement does not argue against clusters. It was shown several times that clusters exist. But our idea influences the

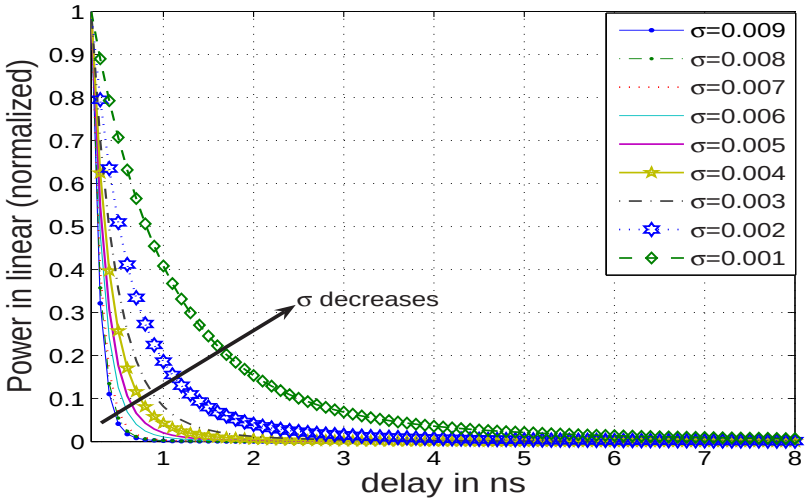

Figure 8: The path dispersion time versus σ with $W = 1GHz$, $\epsilon = 6$.

way clusters are built out of sets of MPCs. If each MPC has a certain time dispersion the PDP of a single reflection looks like the PDP of a cluster.

10.2 Channel model description and parameter estimation

10.2.1 Channel Model Description

Although there are both frequency domain and time domain models that may be appropriate for UWB systems, authors in [55,56] chose to focus on evaluating continuous time domain models. The following expression of the channel impulse response is used:

$$h(t) = \sum_{l=1}^{L} g_l(t)u(t-\tau_l), \tag{31}$$

$$g_l(t) = g_l e^{-(t-\tau_l)/\gamma_l} = \alpha_l e^{-t/\gamma_l} \tag{32}$$

where $\alpha_l = g_l e^{\tau_l/\gamma_l}$.
$g_l(t)$ is used to model the dispersive part and $u(t)$ is the Heaviside function. The signal parameters of the l^{th} MPC are the time delay τ_l, α_l is the complex amplitude, and γ_l denotes the decay constant.

10.2.2 Parameter estimation

At first, the authors of This Section estimated, using a method based on the approximation by regression, the parameter γ_l (it can be seen as the slope of each MPC). Second, they estimated the parameters α_l and τ_l using the SAGE algorithm [52,53]. The number of MPCs L in the observed UWB signal $y(t)$ was derived using the

maximum description length (MDL) algorithm [54] and the *Akaike information criterion* (AIC) [54]. To estimate the parameters α_l and τ_l the SAGE algorithm was exploited [56]. A block diagram summarizing channel estimation parameters is illustrated in Figure 9.

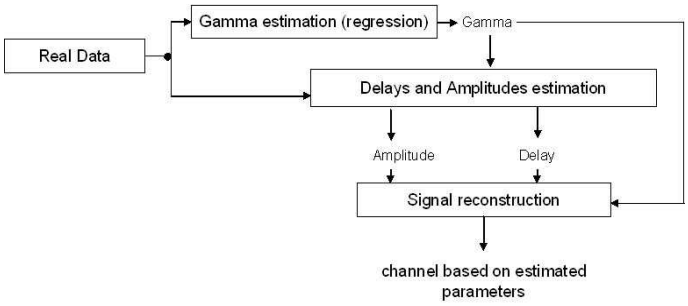

Figure 9: Block diagram describing the estimation of channel model parameters.

10.3 Results

10.3.1 UWB channel model implementation

The analytical channel was implemented, using the Matlab tools [57], on the basis of the equations derived in [48] and [49]. The nature of the environment (dense, number of reflecting/diffracting scatterers, geometry, etc...) is fully parametrizable. For the statistical model, we propose as a first approach to model γ_l, α_l and τ_l using a normal distribution.
Figure 13 shows the power delay profile for simulated analytical channel with $L = 100$, $\bar{\gamma} = 1.5$ and time resolution $0.1667ns$ corresponding $W = 6\ GHz$. These results show that the simulated channel exhibits the same clustered behavior as that evidenced by UWB channel measurements [39].

The PDP is generally characterized by the first central moment (mean excess delay) τ_m and the square root of the second moment (root mean square delay spread), τ_{rms}.

Figure 14 shows the cumulative distribution function of τ_m and τ_{rms} for the analytical channel. These results show that the statistics of the simulated model are in agreement with those published in the literature.

10.3.2 Channel parameters estimation

In this part, we focus on the estimation of the channel parameters using the model based on equation (31). In Figure 16 single realizations of the impulse responses of the analytical channel and the measured channel [39] are shown and compared with the channel built on the basis of our parameter estimates.

The resulting small scale statistics are given in Table 2. These results have been extracted from 500 realizations (in computing these results the power delay profiles

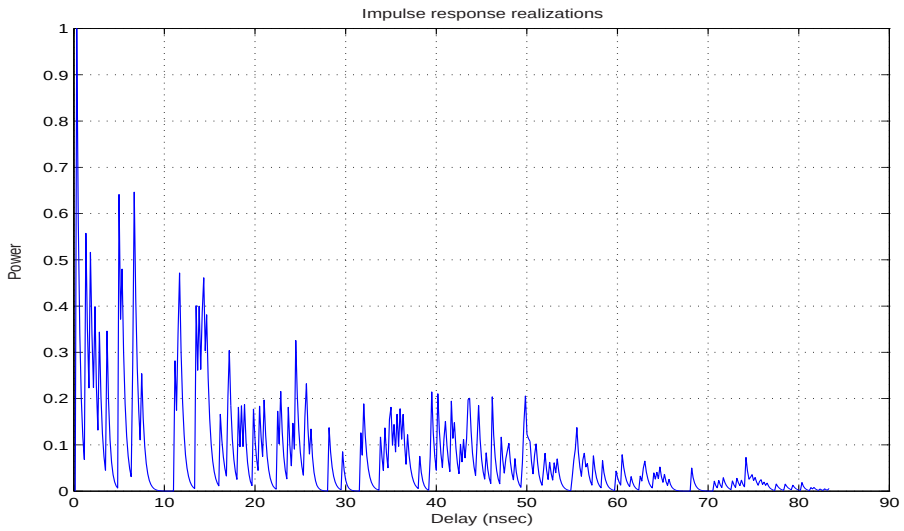

Figure 10: Simulated UWB Channel Impulse Response realization (1) $L = 100$.

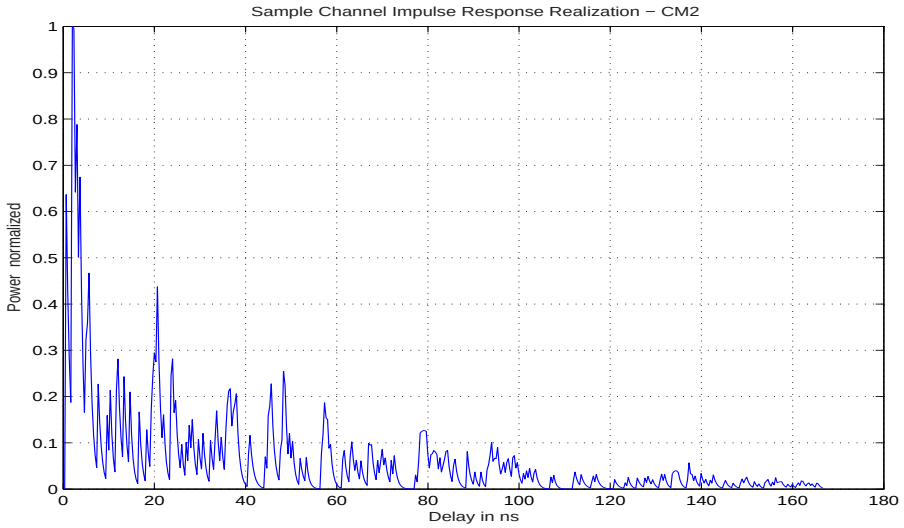

Figure 11: Simulated UWB Channel Impulse Response realization (2) $L = 70$.

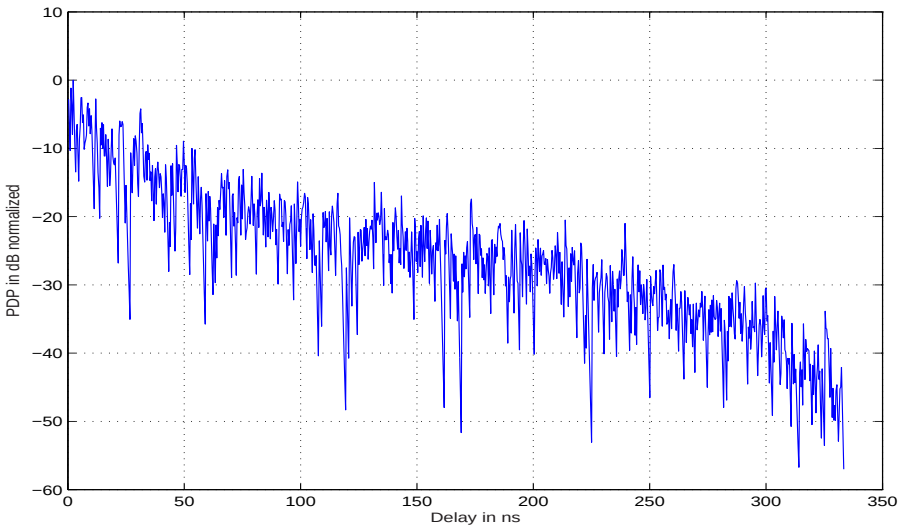

Figure 12: The power delay profile estimated from simulated channel $L = 100$.

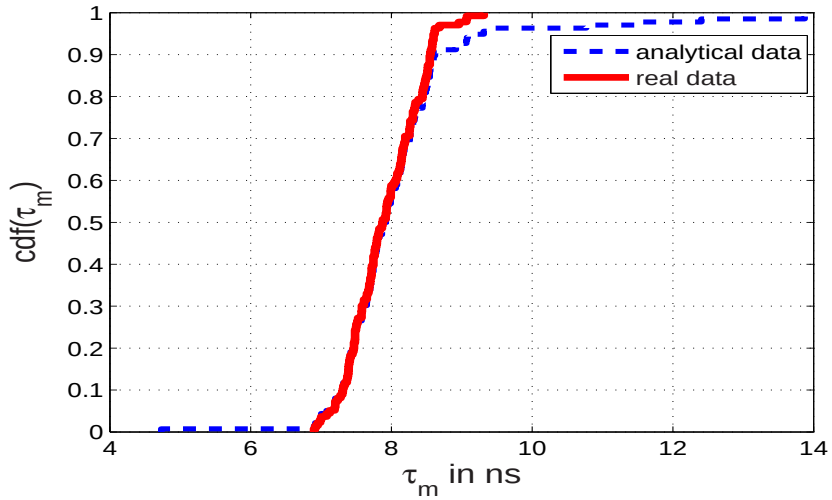

Figure 13: τ_m from simulated analytical channel

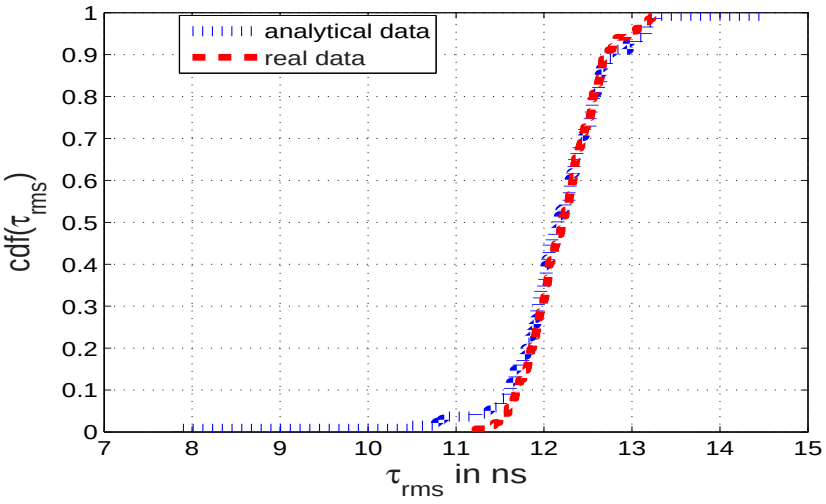

Figure 14: τ_m (top) and τ_{rms} (bottom) both from simulated analytical channel

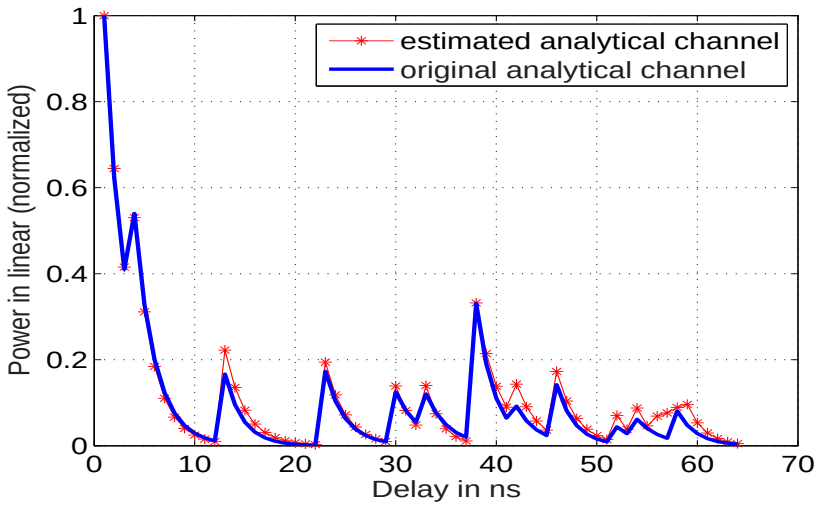

Figure 15: Estimation results for the impulse response of the analytical channel of 1 GHz

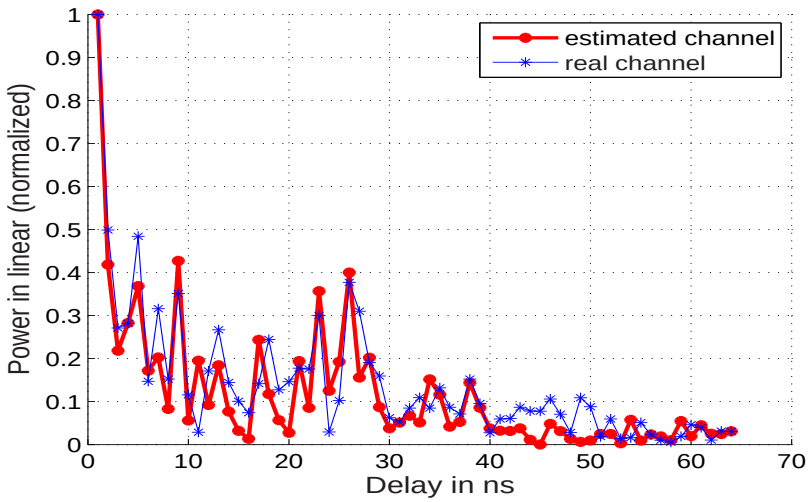

Figure 16: Estimation results for the impulse response of the measured channel for a bandwidth of 1 GHz

Table 2: Small scale statistics

	$\tau_{rms,L=50}$ ns	$\tau_{m,L=50}$ ns	$\tau_{rms,L=100}$ ns	$\tau_{m,L=100}$ ns
mean	11.7953	9.6071	11.3588	8.3215
min	6.0284	2.3504	7.1747	3.6765
max	15.3522	18.4709	14.6920	16.5753

have been normalized). Comparing the results for the different environments reveals some relative trends for the mean excess delay, max excess delay, τ_{rms} delay spread, and the number of paths.

10.4 Conclusion

A novel UWB channel model based on physical propagation effects was introduced. A mathematical description of the model has been discussed and the corresponding parameter extraction presented. The parameter extraction has been based on the SAGE algorithm and some preliminary results have been given. The proposed model presents a good fit to measurement data and is easy to implement. A set of four parameters, namely the number of MPCs, the MPC amplitude, the MPC delay and the MPC decay constant, describes the whole model.

11 Conclusion

This report has illustrated various recent research results about UWB channel modeling. Compared to models presented in Newcom DRB1.2 report [58], new ap-

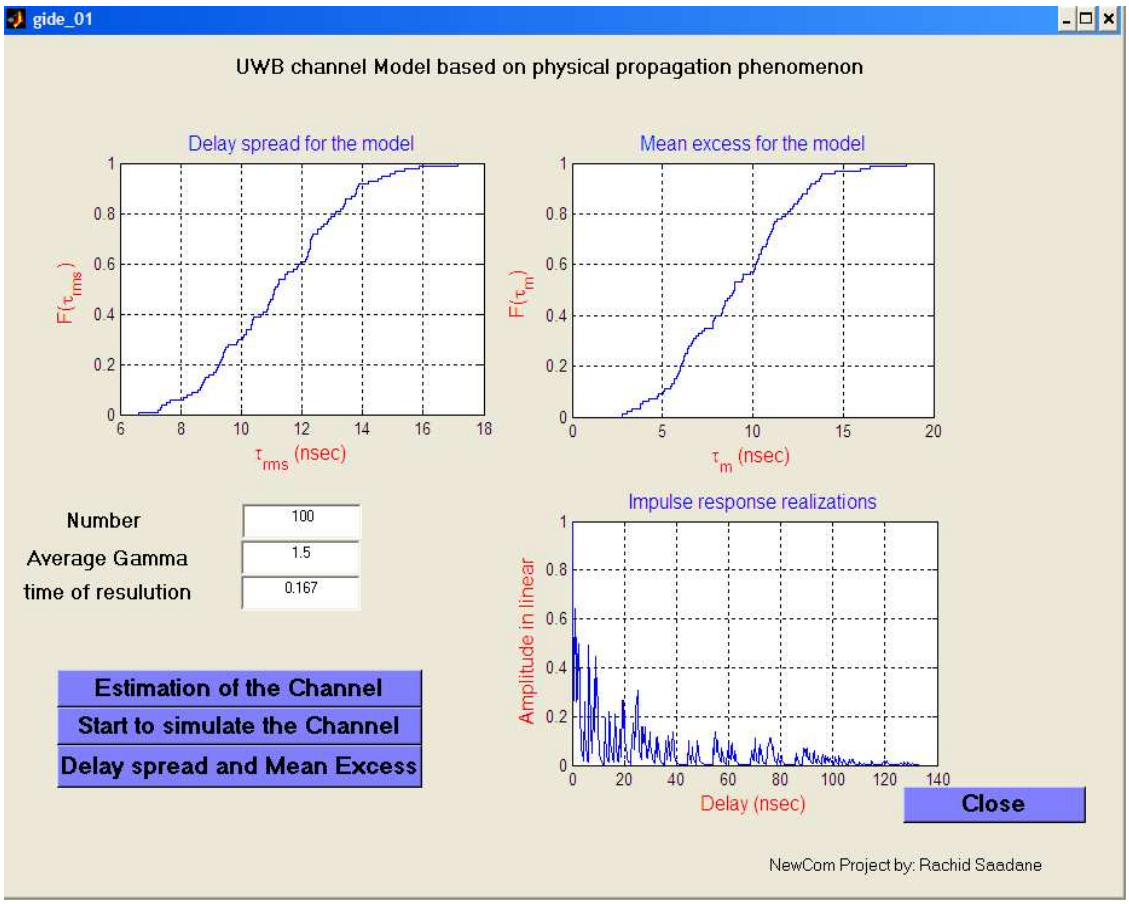

Figure 17: τ_{rms} and τ_m estimation.

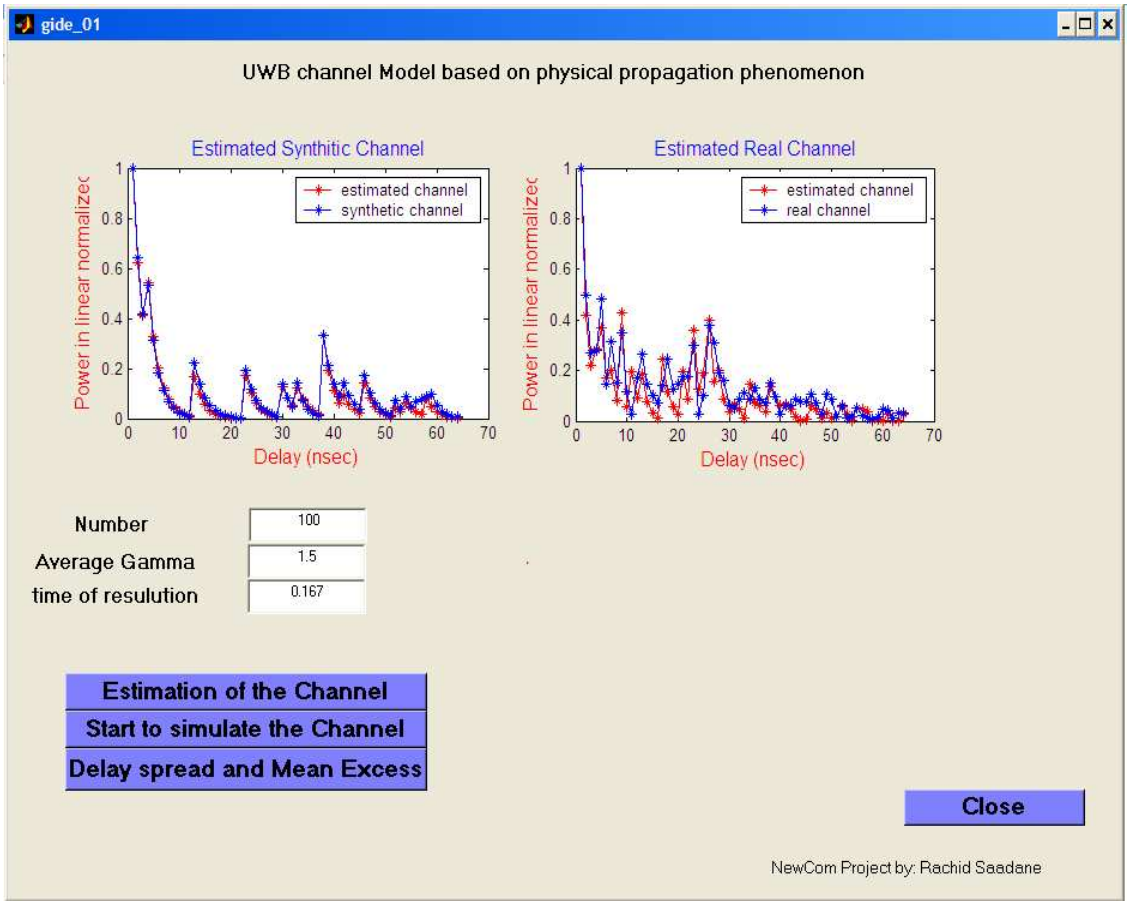

Figure 18: Analytical and real channel parameters estimation.

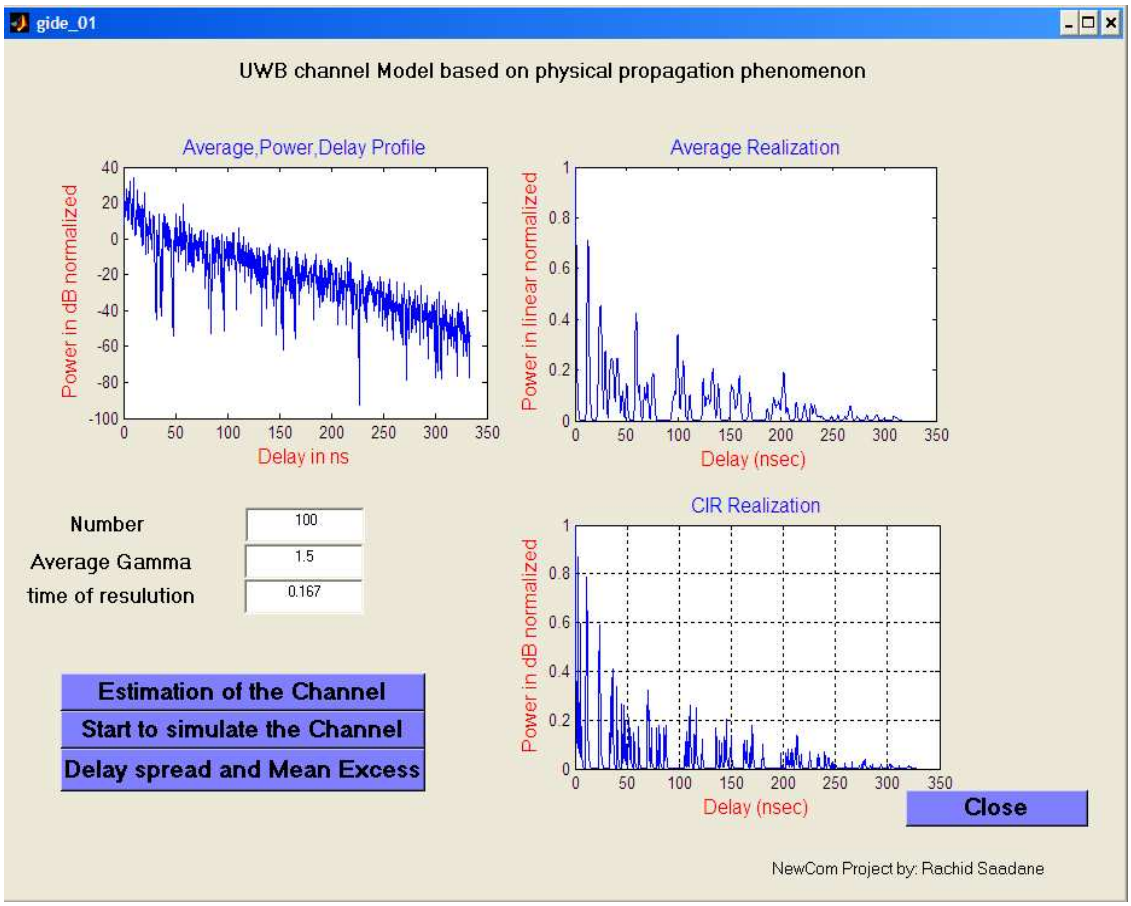

Figure 19: channel simulation based on the proposed model.

proaches were proposed; they are based on information theoretic arguments and on the investigation of UWB propagation mechanisms.

References

[1] Scholtz, R. A. , "Multiple Access with Time-hopping Impulse Modulation," *IEEE Military Communications Conference*, Vol. 2, 11-14 Oct. 1993, pp:447-450.

[2] Win, M. Z. , Scholtz, R. A. , "Impulse radio: how it works "*IEEE Communications Letters*, Vol. 2 Issue: 2, Feb. 1998, pp.36-38.

[3] D. Cassioli, M. Z. Win, and A. F. Molish," The ultra–wide bandwidth indoor channel-from statistical model to simulation," *IEEE Journal on Selected Areas Communications*, vol. 20, 2002 pp. 1247-1257.

[4] J. Kunisch and J. Pamp, "Measurement results and modeling aspects for UWB radio channel", *IEEE Conference Ultra Wideband Systems and Technologies*, 21-23 May 2002, pp. 19-23.

[5] R. Saadane, A. Menouni, R. Knopp,D. Aboutajdine, "Empirical eigenanalysis of indoor UWB propagation channels"*IEEE Global Telecommunications Conference*, November 29-December 3, 2004.

[6] M. Z. Win and R. A. Scholtz, "Impulse Radio: How it works," IEEE Commun. Lett., Vol.2, no.2, pp.36-38, Feburuary 1998.

[7] M. Z. Win and R. A. Scholtz, "Ultra-wide bandwidth time-hopping spread spectrum impulse radio for wireless multiple-access communications," IEEE Trans. Commun., vol.48, pp.679-690, April 2000.

[8] J. Foerster, Evan Green, Srinivasa Somayazulu, David Leeper, "Ultra wideband Techonology for Short or Medium Range Wireless Communications," Intel Technology Journal, 2th Quarter 2001.

[9] H. Zhang, T. Udagawa, T. Arita, and M. Nakagawa, "Home entertainment network: combination of IEEE 1394 and Ultra wideband solutions," 2002 IEEE Conference on Ultra Wideband Systems and Technologies.

[10] C. -C. Chong, Y. Kim and S. -S. Lee, "UWB Channel Model for Indoor Residential Environment," IEEE 802.15-04-0452-01-004a, Sep. 2004.

[11] C. -C. Chong; Y. Kim; S. -Soo Lee; " A modified S-V clustering channel model for the UWB indoor residential environment," VTC 2005-Spring. 2005 IEEE 61st Volume 1, 30 May-1 June 2005 Page(s):58 - 62 Vol. 1

[12] U. G. Schuster and H. Boumlcskei, "Ultra wideband channel modeling on the basis of information-theoretic criteria," *IEEE Transactions on Wireless Communications 2006*, to appear.

[13] R. G. Vaughan and N. Scott, "Super-resolution of pulsed multipath channels for delay spread characterization," IEEE Trans. Commun., vol. 47, no. 3, pp. 343-347, Mar. 1999.

[14] P. A. Bello, Characterization of randomly time-variant linear channels, IEEE Transactions on Communications, vol. 11, pp. 360393, 1963.

[15] H. Linhart and W. Zucchini, Model Selection. New York, NY, USA: Wiley, 1986.

[16] R. B. DAgostino and M. A. Stephens, Eds. , Goodness-of-Fit Techniques. New York, NY, USA: Marcel Dekker, 1986.

[17] J. Keignart and N. Daniele, Channel sounding and modelling for indoor UWB communications, in Proc. Int. Workshop on Ultra Wideband Systems, Oulu, Finland, June 2003.

[18] D. Cassioli, M. Z. Win, and A. F. Molisch, The ultra-wide bandwidth indoor channel: From statistical models to simulations, *IEEE Journal on Selected Areas in Communications*, vol. 20, no. 6, pp. 12471257, Aug. 2002.

[19] W. R. Braun and U. Dersch, A physical mobile radio channel model, *IEEE Transactions on Vehicular Technology*, vol. 40, no. 2, pp. 472482, May 1991.

[20] A. Muqaibel, A. Safaai-Jazi, A. Attiya, B. Woerner, S. Riad, Path-loss and time dispersion parameters for indoor UWB propagation," Wireless Communications, IEEE Transactions on, vol.5, no.3pp. 550- 559, March 2006

[21] V. Hovinen, et al. , "Ultra wideband indoor radio channel models: Preliminary results," in Proc. IEEE Conference on Ultra Wideband Systems and Technologies, pp. 75-79, May 2002.

[22] A. Saleh and R. A Valenzuela, "A statistical model for indoor multipath propagation," *IEEE J. Select. Areas Commun.*, vol. 5, no. 2, pp. 128-137, Feb. 1987.

[23] T. S. Rappaport, "Characterization of UHF multipath radio channels in factory buildings," *IEEE Trans. Antennas Propagat.*, vol. 37, no. 8, pp. 1058-1069, Aug. 1989.

[24] T. K. Sarkar, Z. Ji, K. Kim, A. Medour, and M. Salazar-Palma, "A Survey of Various Propagation Models for Mobile Communication", Antennas and Propagation Magazine, Vol. 45, No. 3, June 2003.

[25] Y. Wang, S. Safavi-Naeini, and S. K. Chaudhuri, "A Hybrid Technique Based on Combining Ray Tracing and FDTD Methods for Site-Specific Modelling of Indoor Radio Wave Propagation," *IEEE Transactions on Antennas Propagation,* Vol. AP-48, No. 5, pp. 743-754, May 2000.

[26] A. M. Attiya and A. Safaai-Jazi, "Simulation of Ultra-Wideband Indoor Propagation", *Microwave and Optical Technology Letters,* V ol. 42, No. 2, July 20 2004.

[27] A. Fort, C. Desset, J. Ryckaert, P. Doncker, L. Biesen and S. Donnay, "Ultra Wide-band Body Area Channel Model", *IEEE International Conference on Communications,* Vol. 4, 16-20 May 2005.

[28] B. Kannan et al. , "UWB channel characterization in office environments," *Tech. Rep. Document IEEE* 802.15-04-0439-00-004a, 2004.

[29] Y. Hao and C. J. Railton, "Analyzing Electromagnetic Structures with Curved Boundaries on Cartesian FDTD Meshes", *IEEE Transactions on Microwave Theory & Techniques,* Vol.46, No.1, pp.82-8, Jan. 1998.

[30] Y. Zhao, Y. Hao, A. Alomainy, C. Parini, "UWB on-body radio channel modeling using ray theory and subband FDTD method" *Microwave Theory and Techniques, IEEE Transactions on* Volume 54, Issue 4, June 2006 Page(s): 1827 - 1835.

[31] A. F. Molisch, K. Balakrishnan, , D. Cassioli, C. -C Chong, S. Emami, A. Fort, J. Karedal, J. Kunisch, H. Schantz, K. Siwiak, "A Comprehensive Model for Ultrawideband Propagation Channels", *IEEE Global Telecommunications Conference (GLOBECOM),* Vol. 6, pp. 3648-3653, November 2005.

[32] G. Kadel and R. Lorenz, "Impact of the radio channel on the performance of digital mobile communication systems," in Proc. *IEEE Int. Symp. on Personal, Indoor and Mobile Radio Communications (PIMRC)'95,* pp. 419-423, 1995.

[33] J. -P. Rossi, "Influence of measurement conditions on the evaluation of some radio channel parameters," *IEEE Trans. on Vehicular Technology,* vol. 48, pp. 1304-1316, 1999.

[34] G. L. Stueber, "Principles of Mobile Communication. " Kluwer, 1996.

[35] B. Kannan et al. , "UWB channel characterization In office environments," *tech. Rep. Document IEEE,* 802. 15-04-0439-00-004a, 2004.

[36] S. Emami et al. Tech. Rep. Document, 2005.

[37] A. F. Molisch, "UWB propagation channels," in UWB communications systems UWB a comprehensive overview" T. Kaiser, ed. , p. in press, *Eurasip,* 2004.

[38] T. S. Rappaport, S. Y. Seidel, and K. Takamizawa, "Statistical channel impulse response models for factory and open plan building radio communication system design," *IEEE Trans. Comm.* , vol. 39, pp. 794-807, 1991.

[39] A. Menouni Hayar, R. Knopp, R. Saadane, "Subspace analysis of indoor UWB channels ", *EURASIP Journal on applied signal processing, special issue on UWB - State of the art,* Vol. 2005 Issue 3 , pp 287-295.

[40] R. L. de Lacerda Neto, A. Menouni Hayar, M. Debbah, B. Fleury, "H A maximum entropy approach to ultra-wideband channel modeling," *IEEE ICASSP 2006,* May 2006, pp: 14-19.

[41] E. T. Jaynes, Probability Theory: The Logic of Science, Cambridge, 2003.

[42] G. L. Bretthorst, Bayesian Spectrum Analysis and Parameter Estimation, Ph.D. thesis, Wahsington University, St. Louis, 1987.

[43] W. H. Weedon, and C. M. Rappaport, "A General Method for FDTD Modelling of Wave Propagation in Arbitrary Frequency Dispersive Media", *IEEE Transactions on Antennas and Propagation,* Vol. 45, No. 3, March 1997.

[44] R. G. Vaughan and N. Scott, "Super-resolution of pulsed multipath channels for delay spread characterization," *IEEE Trans. Commun.* , vol. 47, no. 3, pp. 343-347, Mar. 1999.

[45] M. Pendergrass, IEEE P802. 15 Working group, "Empirically Based Statistical Ultra- Wideband Channel Model," April 2002.

[46] J. M. Cramer, R. A. Scholtz, M. Z. , Win, " Spatio-temporal diversity in ultra wideband radio," *Wireless Communications and Networking Conference, IEEE,* Vol. 2, pp. 888-892, 1999.

[47] R. C. Qiu, "A Study of the Ultra-Wideband Wireless Propagation Channel and Optimum UWB Receiver Design," *IEEE Journal on Selected Area in Communications,* vol. 20, No: 9, December 2002.

[48] R. C. Qiu, "A Generalized Time Domain Multipath Channel and Its Application in Ultra-Wideband (UWB) Wireless Optimal Receiver DesignPart II: Physics-Based System Analysis," *IEEE Trans. on Wireless Comm.,* vol. 3, No: 6, November 2004.

[49] P. R. Barnes, "On the Direct Calculation of a Transient Plane Wave Reflected from a Finitely Conducting Half Plane," *IEEE Trans. on Electromagnetic Compatibility,* Vol. :33, No: 2, MAy 1991.

[50] A. F. Molisch, J. R. Foerster, M. Pendergrass, "Channel models for ultra-wideband personal area networks, "*IEEE Wireless Communications,* Vol. 10, Issue 6, Dec. 2003 pp. 14 – 21.

[51] A. F. Molisch, " Ultrawideband propagation channels - theory, measurement,and models, " (invited paper) *IEEE Trans. Vehicular Techn. ,special issue on UWB,* in press, 2005.

[52] J . A. Fessler and A. 0. Hero, Complete-data spaces and generalized EM algorithms, in Plac. IEEE Conf. Acoust. , Speech, Signal Processing, vol. 4, 1993, pp. 1-4.

[53] B. H. Fleury and M. Tschudin and R. Heddergott and D. Dahlhaus and K. L. Pedersen, "Channel parameter estimation in mobile radio environments using the SAGE algorithm," *IEEE-JSAC,* Oct 1999, vol. 17, No. 3, pp. 434–450.

[54] R. Saadane, A. Menouni Hayar, R. Knopp, D. Aboutajdine, "On the estimation of the degrees of freedom of in-door UWB channel," *VTC Spring'05,* 29th May - 1st June, 2005.

[55] R. Saadane, D. Aboutajdine, A. Menouni Hayar, "A statistical UWB channel model based on physical analysis," aict-iciw, pp. 80, Advanced International Conference on Telecommunications and International Conference on Internet and Web Applications and Services (AICT-ICIW'06), 2006.

[56] R. Saadane, D. Aboutajdine, A. Menouni Hayar, H. Hofstetter, "Propagation phenomenon Analysis for Statistical UWB channel model" Submitted to VTC Spring 2007.

[57] R. Saadane, A. Hayar Menouni, "Eurecom proposed UWB channel model," http://www.eurecom.fr/ menouni/NewcomProjectB/EurecomUWBChannelModel/.

[58] A. Menouni Hayar, L. Mucchi, G. Vitetta, "Second report on UWB channel models,", Newcom Project B DRB1.2 report, 2005.

[59] D. Porrat, D. N. C. Tse and S. Nacu, "Channel Uncertainty in Ultra Wideband Communication Systems,", Submitted to IEEE Trans. on Information Theory, 2006.